

LPP EUV Conversion Efficiency Optimization

J.R. Hoffman, A.N. Bykanov, O.V. Khodykin,
A.I. Ershov, N.R. Böwering, I.V. Fomenkov, W.N. Partlo, D.W. Myers

Cymer, Inc., San Diego, California, USA

ABSTRACT

Efficient conversion of laser light into EUV radiation is one of the most important problems of the laser-produced plasma (LPP) EUV source. Too low a conversion efficiency (CE) increases the amount of power the drive laser will have to deliver, which, besides the obvious laser cost increase, also increases the thermal load on all the components and can lead to increased debris generation. In order to meet the requirements for a high-volume manufacturing (HVM) tool and at the same time keep the laser power requirements within acceptable limits, a CE exceeding 2.5% is likely to be required. We present our results on optimizing conversion efficiency of LPP EUV generation. The optimization parameters include laser wavelength, target material, and laser pulse shape, energy and intensity. The final choice between parameter sets that leads to the required minimum CE is dependent on the debris mitigation solutions and the laser source available for a particular parameter set.

Keywords: EUV metrology, EUV lithography, laser produced plasma, LPP, conversion efficiency, planar targets, lithium, tin, spectrometer, source spot size, spectral distribution

1. INTRODUCTION

The application of EUV lithography to large-scale semiconductor chip manufacturing requires the availability of a high power EUV radiation source with a narrow line width centered at a wavelength of 13.5nm. The CE of laser light, in the case of an LPP source, or electrical energy, in the case of a discharge produced plasma (DPP) source, to EUV radiation has a direct impact on the capital cost and the cost of ownership of any EUV source. Thus finding the conditions that optimize the CE of a source, while not drastically changing the lifetime, is of fundamental importance to the viability of any source.

It is convenient to describe the LPP CE as energy produced into 2π steradian and 2% bandwidth around 13.5nm divided by the energy of the irradiating laser pulse. The best CE for LPP with Xe liquid jet target irradiated by Nd:YAG laser at 1064 nm was previously reported to be in a 1% range [1]. This number was achieved after a significant effort on optimization of the laser pulse shape and target properties. In particular, it was found that a laser pre-pulse on the target was required. Without a pre-pulse, the CE was only about 0.3-0.4%. In order to make an LPP EUV source viable for HVM tools, CE exceeding 2.5% will likely be required.

In the present paper we are reporting results on CE optimization for LPP source using different thickness lithium and tin foils as well as tin droplets as target materials. Different laser energies (10 mJ to 1 J per pulse), wavelengths (266 nm, 355 nm, 532 nm, and 1064 nm), pulse widths (0.5 ns to 20 ns) and laser intensities (10^9 W/cm² to 10^{12} W/cm²) were used.

2. EXPERIMENTAL SETUP

A detailed description of the diagnostics used in this paper is given in [2]. Therefore, we will only present a brief description of each diagnostic below, followed by a summary of the results obtained. Figure 1 shows two vacuum chamber configurations used to make the measurements. The base pressure in each chamber is typically in the low 10^{-6} Torr range. The drive laser is focused through a calcium fluoride window onto the target material. This port is referenced as zero degrees azimuthal angle, with the positive angle going in the counterclockwise direction. The diagnostics were mounted onto vacuum ports located at fixed angles from the drive laser beam. For the CE measurements on foils, ‘flying circus’ type absolute energy arms were mounted onto the +25, -50 and +75 degree ports. For the CE measurements on droplets, the absolute energy arms were mounted onto the +25, +45 and -45 degree ports. The high-resolution spectrum measurements were taken at -50 degrees relative to the foil target normal.

The ‘flying circus’ type absolute energy arm configuration (see Figure 1) includes an AXUV100 EUV diode, Zr filter and a normal incidence multiplayer mirror.

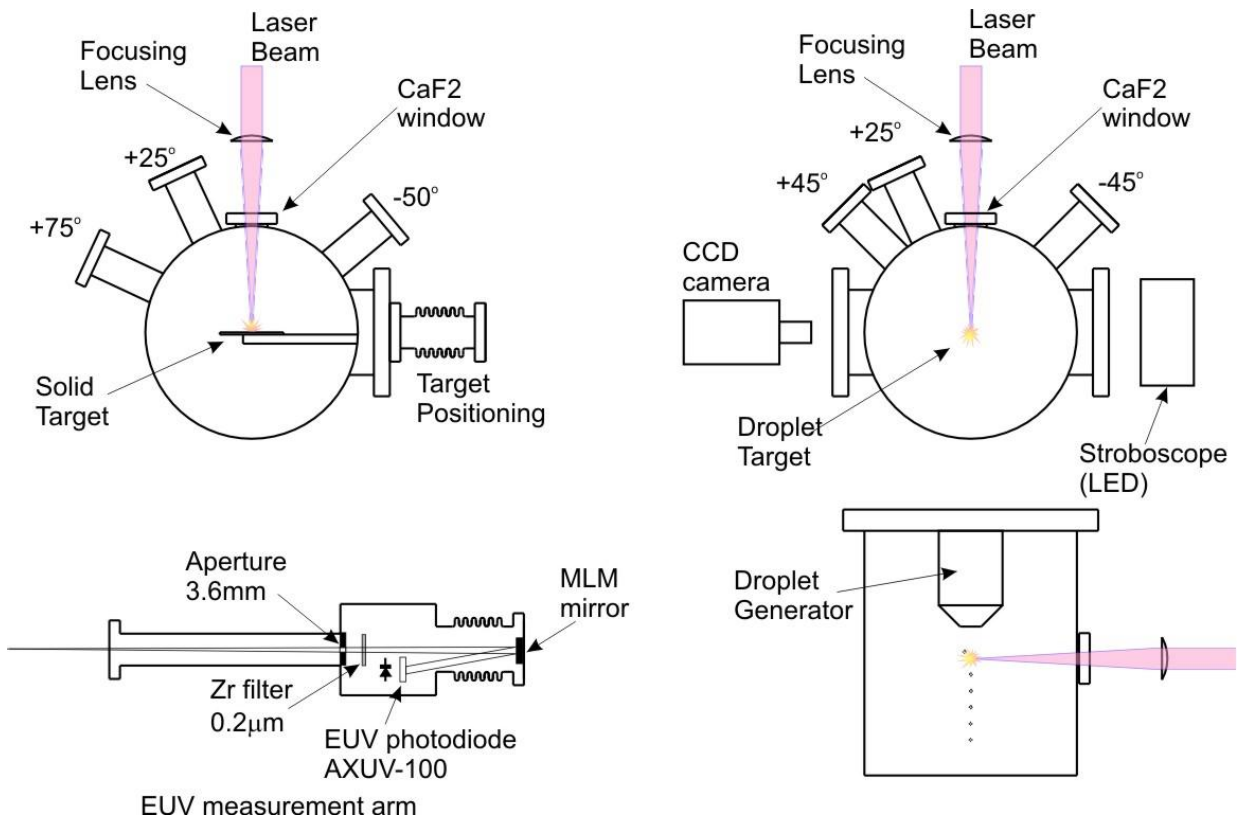


Figure 1. Experimental setups used to measure the angular distribution of the EUV emission from both lithium and tin targets.

The EUV pinhole camera [2] is used for EUV imaging of the LPP source. The EUV pinhole camera consists of a $50 \mu\text{m}$ pinhole, a $0.2 \mu\text{m}$ Zr filter (placed right after the pinhole), a calibrated 45° Si/Mo MLM, and a 512×512 CCD camera.

The droplet generator works either in continuous mode (Continuous Droplet Generator, CDG) or drop-on-demand (DoD) mode [3]. In CDG mode the Sn droplets are generated by stimulating continuous Sn jet with a PZT at typical frequencies in the 10^4 Hz range. In DoD mode the droplets are generated with the frequency of the drive laser (typically

10 Hz) synchronized with the laser triggering circuit. Droplet diameters can be varied in the 30 to 200 μm range. The droplets are monitored by a CCD camera with stroboscopic backlighting. The photograph of an LPP and a stroboscopic image of metal droplets are shown in Figure 2.

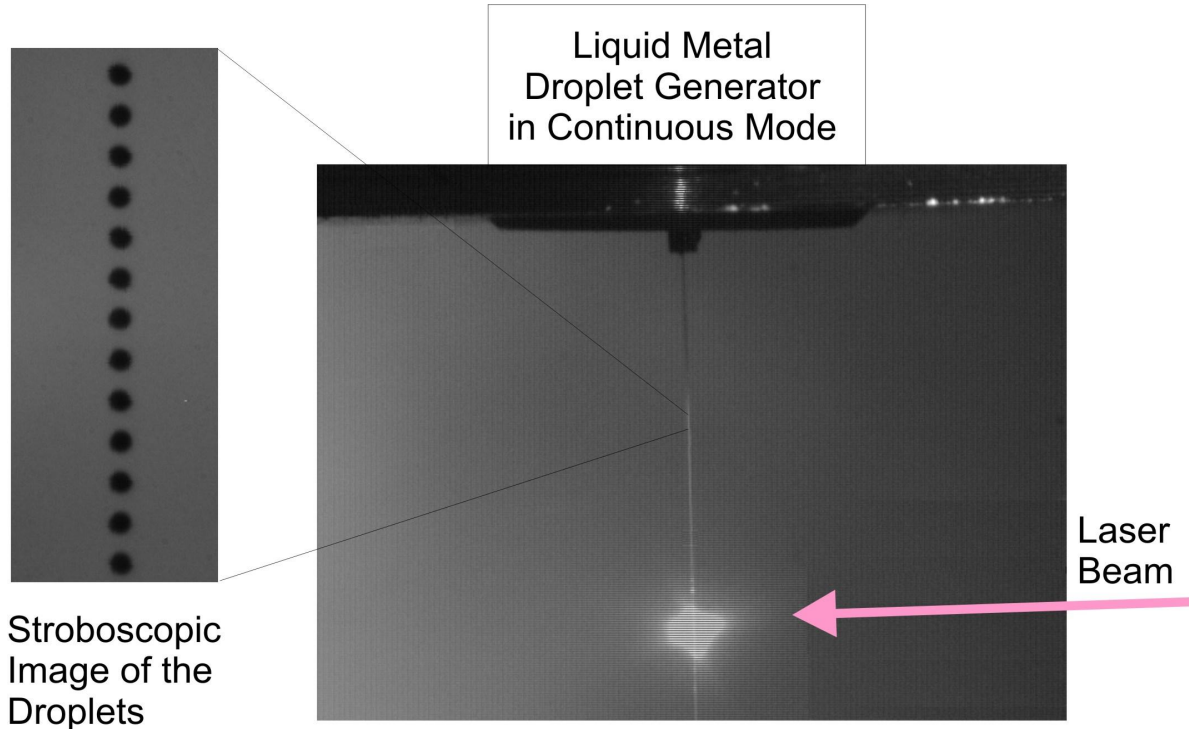


Figure 2. The photograph of LPP and the stroboscopic image of the droplets.

3. MEASUREMENT RESULTS

3.1. HIGH RESOLUTION SPECTRUM MEASUREMENTS

A high-resolution flat field spectrometer [2] was built to look at EUV plasma emission spectra produced in various laser/target combinations. The advantage of this type of spectrometer over scanning grazing incidence spectrometers is that the entire spectrum range is recorded in a single shot.

Figures 3a, 3c, and 4 show the measured spectra of lithium. Figure 3a shows a false color representation of the CCD image of the lithium line spectrum obtained by using a drive laser at 355nm. Binning the y-axis converts the CCD image into the line spectrum shown in Figure 3c. The data in Figure 3c is plotted logarithmically to show more of the structure in the spectra. The full width half maximum of the 13.5nm is less than the resolution of the spectrometer, or < 30pm. The implication of this is that the lithium line falls easily within the 2% bandwidth of the multilayer mirrors. Figure 4 shows how the spectra are used to confirm that the optimum CE for a particular parameter set has been reached. If the plasma is under heated, longer wavelength lines are bright, and if the plasma is overheated, shorter

wavelength lines start to appear and the line ratios change. If we see these characteristics in the measurements, then the optimum has been found.

Figures 3b, 3d, and 5 show the spectral results for tin illuminated with 1064nm laser light. The tin unresolved transition array (UTA) is clearly visible as the bright, broad peak centered on 13.5nm. Figure 5 shows how the central peak changes, as the tin plasma is first under heated, pass through the optimum, and then overheated. Interestingly, the center wavelength changes very slightly with the laser intensity, unlike the brightness of the line.

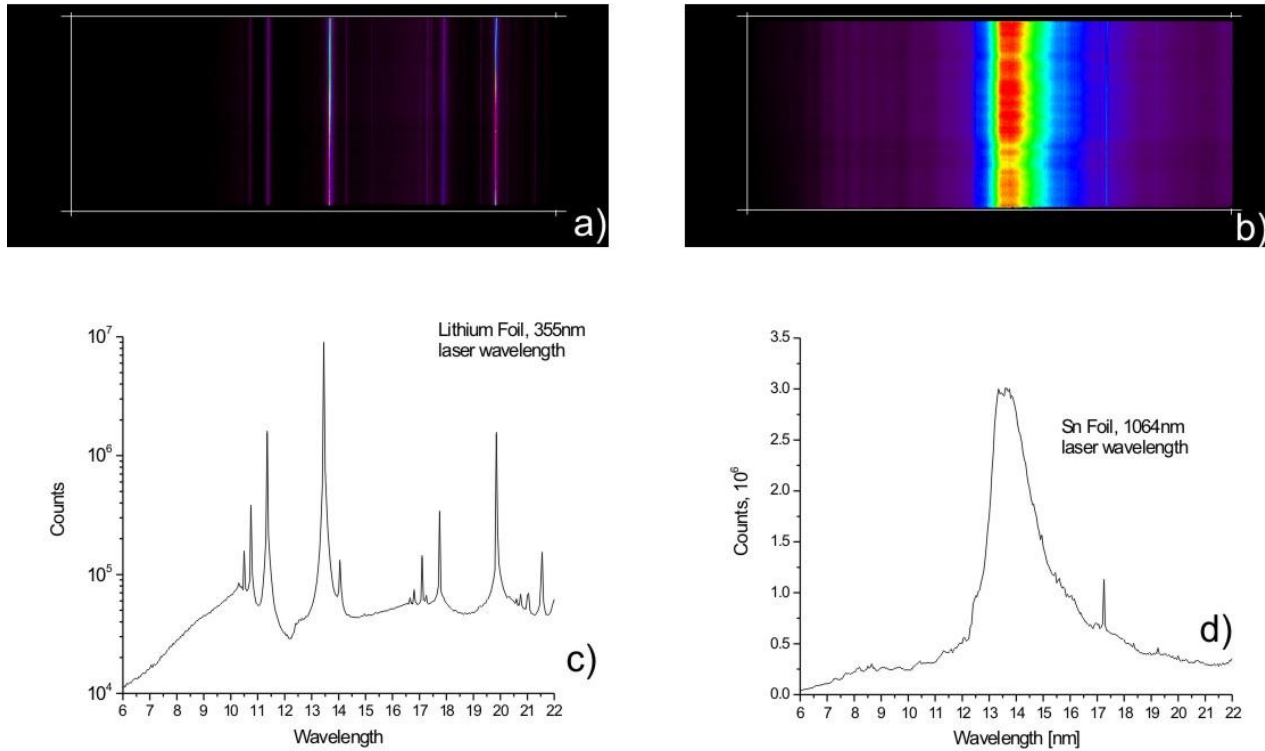


Figure 3. Spectra measured with high-resolution flat-field grazing incidence EUV spectrometer. a), b) False color images of raw data recorded by the CCD camera for lithium foil (355 nm laser) and tin foil (1064 nm laser) correspondingly; c) lithium spectrum graph; d) tin spectrum graph.

3.2. EUV PINHOLE CAMERA MEASUREMENTS OF THE SOURCE SIZE

The EUV camera images were analyzed using a program written in the IDL programming language. The algorithm used to analyze the image was as follows: 1) the 355nm image data were rotated by -45 degrees, and the 1064 nm image data were rotated by -60 degrees, to align the image horizontal with the XY axes; 2) next, an ellipse was fit to the full width half max (FWHM) contour of the image. The calculated fit parameters for the ellipse then give the xy and z extent of the source.

Figure 6 shows an example of the source size measurements on a lithium target. The trend shown in Figure 7 is that the EUV source size increases with the drive laser intensity. Table 1 shows a summary of measured source sizes at the best CE laser intensities. The results show that for lithium, the source size depends weakly on the laser energy, but strongly on the laser wavelength. For all cases, the source size is well within the maximum etendue limits of the collection optics. The data shows that for longer wavelengths, the source size increases, nearly doubling when going

from a laser wavelength of 355 nm to 1064 nm. This supports current theoretical models [4], which predict that shorter wavelength radiation penetrates deeper into the expanding plasma before it is completely absorbed, whereas the longer wavelength radiation is absorbed closer to the surface.

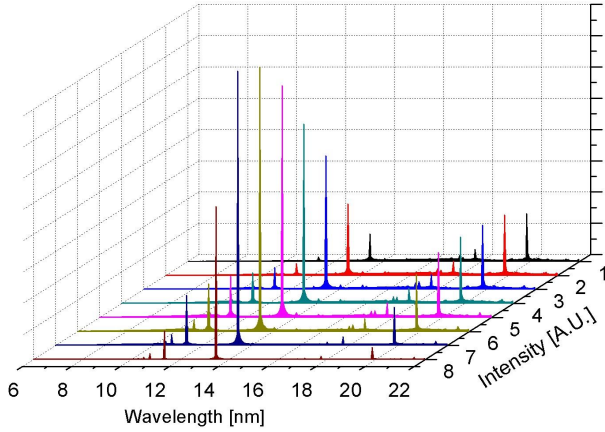


Figure 4. 3D plot of the Lithium spectrum as a function of laser Intensity.

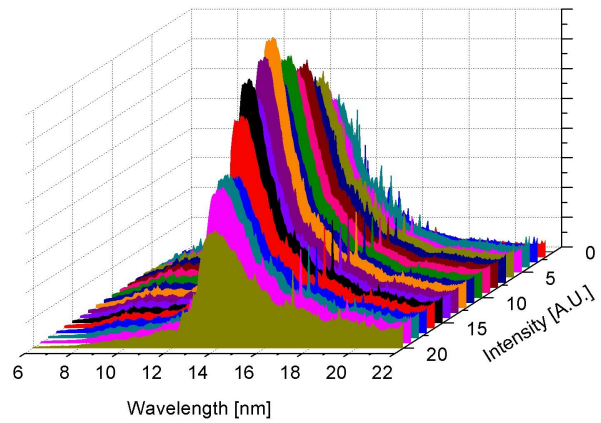


Figure 5. 3D plot of the Tin spectrum as a function of laser Intensity.

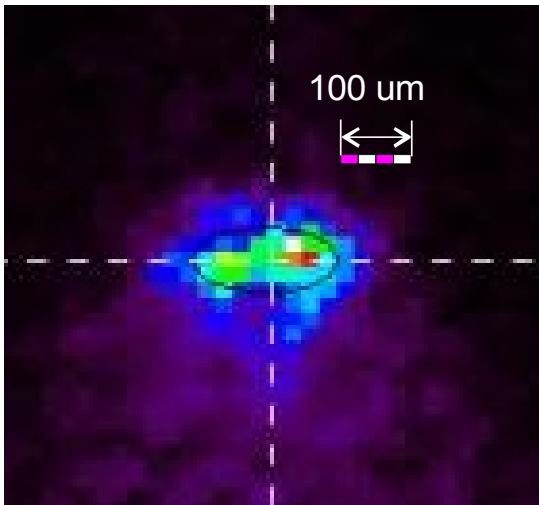


Figure 6. False color image obtained from the pinhole CCD camera for lithium foil target and 355 nm drive laser.

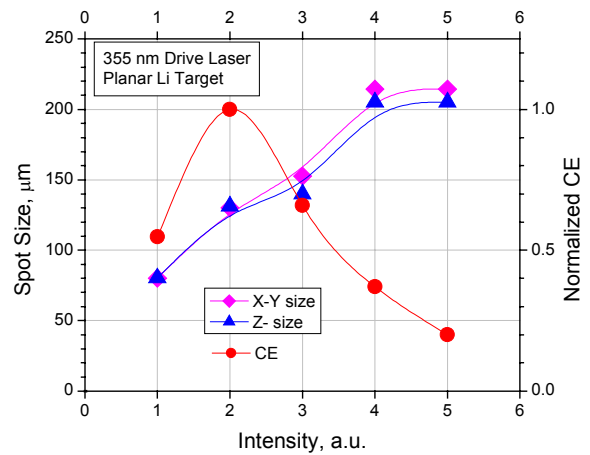


Figure 7. Variation of the source size produced by lithium foil targets versus laser intensity. XY is the plane normal to the laser beam that propagates along Z-axis.

Laser Wavelength	355nm		1064nm	
Drive Laser Energy	E_0	$2E_0$	E_1	$2E_1$
Best CE	2.3%	2.5%	2.5%	2.6%
XY Source Size at best CE	~125um	~130um	~200um	~225um
Z Source Size at best CE	~125um	~120um	~190um	~120um

Table 1. Summary of EUV source size measurements for a planar Lithium target

3.3. ANGULAR DISTRIBUTION OF CE

Figure 8 shows an example of the measured CE versus the laser intensity from a planar target of lithium illuminated by 355nm laser radiation. Notice that as the laser intensity increases, the CE increases until it reaches a maximum. According to these measurements, significant non-uniformity of CE is observed for lithium, thus the total collected power calculation for HVM tool will have to take this into account.

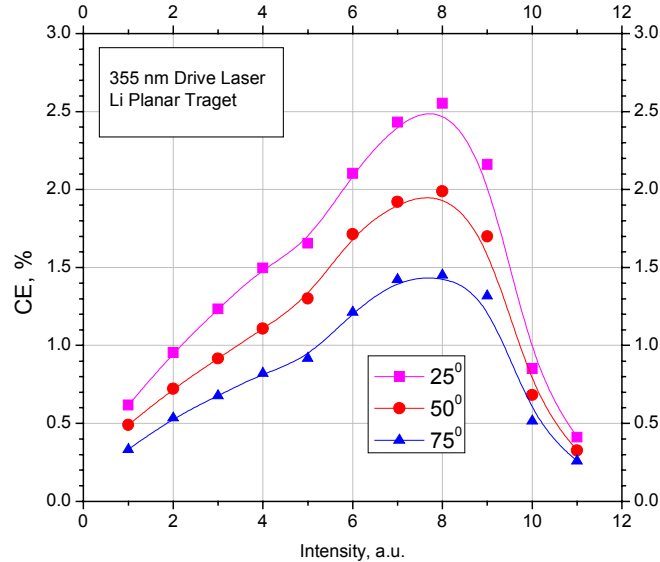


Figure 8. CE measured at three different directions with respect to the laser beam versus laser intensity for planar Li target.

Measurement of angular distribution for Sn targets in both planar and spherical geometries are presented in Figures 9 and 10 respectively. Both geometries demonstrate fairly uniform CE distribution for Sn unlike Li targets.

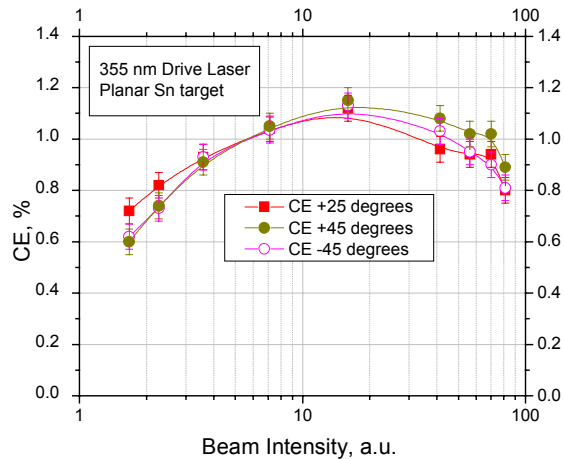


Figure 9. Angular CE distribution for Sn solid target. Drive laser has a wavelength of 355 nm.

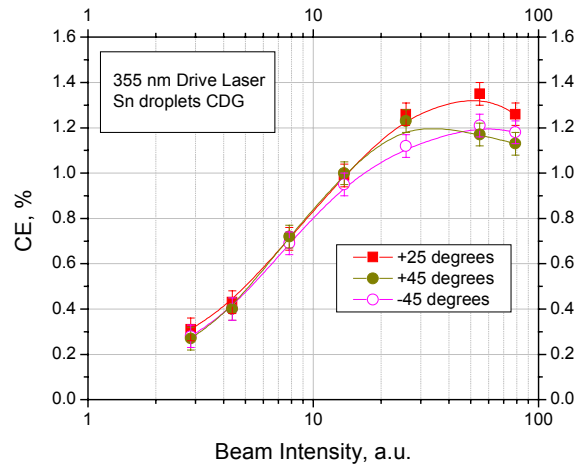


Figure 10. Angular CE distribution for Sn droplet target (continuous droplets). Drive laser has a wavelength of 355 nm.

The angular measurement results for various targets are summarized in the Table 2.

Laser Wavelength	Li foil		Sn Target	45° : 25°
	50° : 25°	75° : 25°	Plate	Droplets
355 nm	0.75	0.68	~1	~1
1064 nm	0.58	0.42	TBD	TBD

Table 2. CE angular distribution.

3.4. MEASUREMENT OF CE WITH PRE-PULSE

The first experiments with a laser pre-pulse on tin droplets revealed CE increase at a delay time on the order of 400 μ s (Figure 11). In this experiment, a second YAG laser was used to generate a pre-pulse with pulse energy being a small fraction of that for the main pulse. The increase is approximately 20% as compared to the CE measurements without pre-pulse. The observed increase for tin is significantly less than that measured for frozen Xe targets [1].

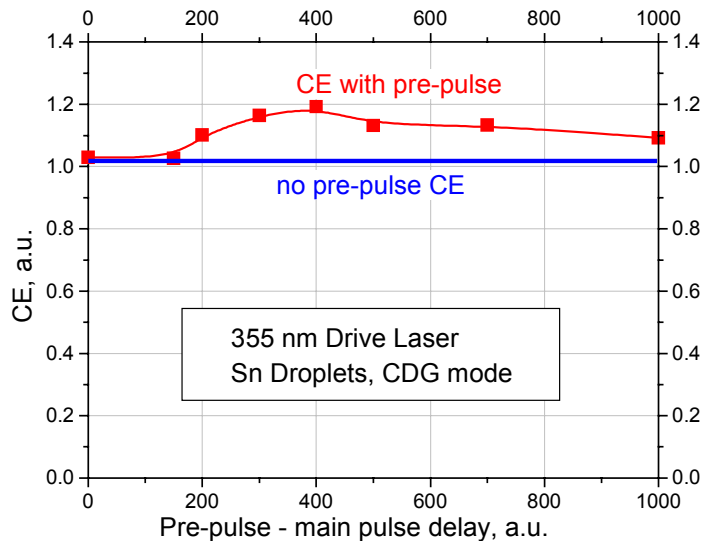


Figure 11. Results of first experiments on pre-pulse CE optimization.

3.5. CE OPTIMIZATION FOR TIN TARGETS

Since tin spectrum consists of a large number of different transitions, optimizing laser/target conditions allows stimulating transitions within the 13.5nm band. Figure 12 shows high-resolution spectra of tin plasma in four different laser conditions. The maximum CE values we have achieved are 3 – 5%.

4. CONCLUSIONS

We have tested various laser wavelengths, pulse widths, energies, and target material combinations to find the optimal conversion efficiency. It has been shown that lithium produces narrow line emission with CE in excess of 2% when used with XeF laser. Lithium spectrum is well suited for use with Mo/Si multi-layer mirrors and much narrower than the 2% bandwidth requirement. The source size of the lithium emission has been shown to be small, and will easily meet the etendue requirements for efficient collection of the emitted light. The source size has a strong dependence on the drive laser wavelength and a weak dependence on the drive laser energy.

The angular distribution measurements revealed better uniformity for tin than for lithium. Comparison of different target geometries revealed increased CE for Sn droplets in comparison to the planar targets. Pre-pulse leads to the noticeable increase in CE. Additional work on pre-pulse optimization is planned.

The conversion efficiency is only one consideration among many for the appropriate choose of drive laser parameters and target material. Ultimately, the initial cost and the cost of operation of the high volume manufacturing tool will dictate which laser/target combination is the best. System tradeoffs might require choosing lower CE options to extend collecting optics lifetimes.

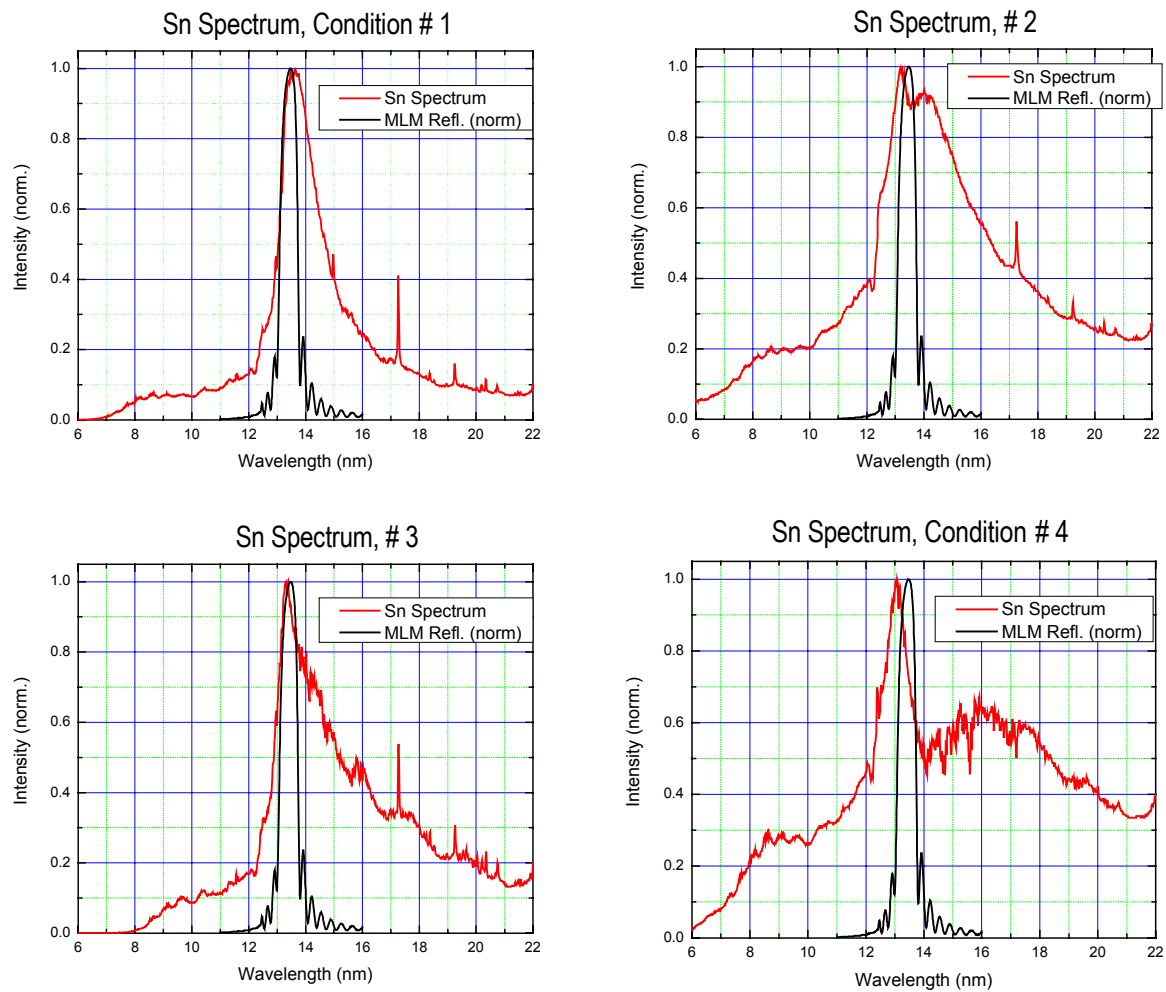


Figure 12. Tin plasma spectra for four different laser radiation conditions.

5. REFERENCES

1. G Kooijman, R. de Bruijn, K. Koshelev, F. Bijkerk, W. Shaikh, A. J. Bodey, G. Hirst, "Prepulse enhanced EUV yield from a xenon gas-jet laser produced plasma". Central Laser Facility Annual Report 2001/2002, p142-144.
2. N. R. Böwering, J. R. Hoffman, O. V. Khodykin, C. L. Rettig, B. A. M. Hansson, A. I. Ershov, I. V. Fomenkov Metrology of laser-produced plasma light source for EUV lithography. Proceedings of SPIE XIX Metrology Conference. Santa Clara, 27 Feb-04 Mar 2005, #5752-144.

3. J. M. Algots, O. E. Hemberg, A. N. Bykanov. Liquid metal micro-droplet generator for laser produced plasma target delivery used in an extreme ultra-violet source. Proceedings of SPIE IX Emerging Lithographic Technologies Lithography Conference. Santa Clara, 27 Feb-04 Mar 2005, #5751-108.
4. J. J. MacFarlane, C. Rettig, I. E. Golovkin, P. R. Woodruff, P. Wang. Radiation-hydrodynamics, spectral, and atomic physics modeling of laser-produced plasma EUVL light sources. Proceedings of SPIE IX Emerging Lithographic Technologies Lithography Conference. Santa Clara, 27 Feb-04 Mar 2005, #5751-68.